Supplementary Material

Sulfur doped Porous Carbon Sheets Embedded with Rich Iron Sites for the $^1O_2$ Dominated Peroxymonosulfate Activation

Yadan Song [a], Yalong Liu [a], Yangju Li [a*], Haipeng Hu [a], Kexin Huang [a], Zhe Zhang [a], Zhongxian Li[c*], Wanning Cao [b], Kai Jiang [a], Dapeng Wu [a*]

[a] *School of Environment, Henan Normal University, Key Laboratory of Yellow River and Huai River Water Environment and Pollution Control, Ministry of Education, Xinxiang, Henan 453007, PR China.*

[b] *Collaborative Innovation Center of Henan Province for Green Manufacturing of Fine Chemicals, Key Laboratory of Green Chemical Media and Reactions, Ministry of Education, School of Chemistry and Chemical Engineering, Henan Normal University, Xinxiang, Henan 453007, PR China.*

[c] *Henan Acad Sci, High & New Technol Res Ctr, Zhengzhou 450002, Henan, Peoples R China*

[*] *Corresponding author. E-mail address: dapengwu@htu.edu.cn (Dapeng Wu), liyangju@hut.edu.cn (Yangju Li), lzxnew337@126.com (Zhongxian Li)*

Table S1 The analytical conditions of Phenol, BPA, TC, and SMX. The HPLC was equipped with C-18 chromatographic column and a UV detector.

Organics	mobile phase (v/v)	Flow rate (mL/min)	Detection wavelengtl (nm)
Phenol	Methanol/Water = 70/30	1	270
BPA	Methanol/Water = 60/40	1	230
TC	Methanol/0.1% Methanoic acid = 25/75	1	355
SMX	Acetonitrile/0.2% Methanoic acid = 30/70	1	270

Table S2 BET surface area, pore properties of catalysts.

Samples	BET surface are: (m²/g)	Pore volume (cm^3/g)	Pore size (nm)
N–C	544.80	0.42	3.06
Fe–NC	537.75	0.54	4.01
Fe–SNC–0.2	509.89	0.53	4.01

Table S3 The surface elemental composition and content of Fe–NC and Fe–SNC–0.2.

Samples	**XPS (at.%)**				
	C	N	O	Fe	S
Fe–NC	74.30	15.57	10.00	0.50	0
Fe–SNC–0.2	75.56	16.29	7.10	0.54	0.51

Table S4 The fitting results for the N 1s spectra of Fe–NC and Fe–SNC–0.2.

Samples	**XPS (at.%)**			
	Fe–Nx	pyridinic N	graphitic/pyrrolic N	Oxidized N
Fe–NC	28.14	51.66	8.55	11.66
Fe–SNC–0.2	24.53	49.25	11.55	14.67

Table S5 Parameters of Xinxiang natural surface water collected from Weihe River.

Parameter	Water matrices	
	Weihe river	Tap water
pH	8.45	7.56
BOD_5 (mg/L)	12.83	0.36
COD (mg/L)	22.57	1.28
TDS (mg/L)	694	132
TN (mg/L)	1.02	0.005
TP (mg/L)	0.12	N.D.

N.D.: not detected.

Table S6 The percentage of each component in XPS spectra before and after reaction.

Samples	XPS (at.%)				
	C	N	O	Fe	S
Before reaction	75.56	16.29	7.10	0.54	0.51
After reaction	79.58	7.85	11.83	0.4	0.34

Table S7 The percentage of each component in S 2p before and after reaction.

Samples	XPS (at.%)	
	Oxidized-S groups	C-S-C
Before reaction	69.61	30.39
After reaction	73.37	26.63

Table S8 The percentage of each component in N1s before and after reaction.

Samples	**XPS (at.%)**			
	Fe–Nx	pyridinic N	graphitic/pyrrolic N	Oxidized N
Before reaction	24.5	49.25	11.55	14.67
After reaction	23.3	48.40	11.20	17.02

Table S9 The percentage of each component in Fe 2p before and after reaction.

Samples	XPS (at.%)		
	Fe^0	Fe(II)	Fe(III)
Before reaction	19.56	49.39	31.05
After reaction	34.43	39.38	26.19

Table S10 Comparison of different oxidative degradation techniques of phenol in the last two years.

Degradation methods	Contaminant	Removal efficiency (%)	η_{TOC} (%)	k (min^{-1})	Ref.
Photoelectrochemical	Phenol	96 (120 min)	/	0.035	1
UV-ZnO	Phenol	99 (150 min)	/	/	2
UV-H_2-Rh/WO_3	Phenol	100 (180 min)	27.6 (180 min)	0.0018	3
O_3-RPB	Phenol	100 (10 min)	96.42 (30 min)	/	4
UV-H_2O_2-CoP/Fe^{2+}	Phenol	80 (120 min)	/	/	5
PMS/Fe-SNC-0.2	Phenol	99 (10 min)	92 (20 min)	0.3569	This work

In order to successfully combat pathogenic microorganisms in wastewater and safeguard ecosystems and public health, wastewater treatment plants typically employ chlorination and ozonation as their last stage [6]. However, the reactions of chlorine with organic matters from the wastewater result in the formation of disinfection by-products (DBPs), which contribute to the overall toxicity of the wastewater and may affect potential reuse. Ozone is a disinfectant that can be used instead of chlorine to inactivate pathogens that are resistant to chlorine in drinking water and reduce the toxicity of wastewater [7]. Wert et al. have shown that ozone was capable of reducing DBPs formation potential by at least 20% [8]. Ozone-based advanced oxidation processes show promise for these pollutants' removal, but the mineralization via ozonation alone is unsatisfactory and not cost-effective.

Table S11 Comparison of catalysts derived from MOFs for PMS activation.

Catalyst (loading, g/L)	PMS (g/L)	Contaminant	C_0 (mg/L)	Removal efficiency	TOF ($g^{-1}min^{-1}$)	Ref.
NPC_{ZIF-8}(0.2)	0.5	Phenol	20	100% (50 min)	0.395	9
SNG-0.3(0.2)	2	Phenol	20	100% (90 min)	0.215	10
5%Fe-g-C_3N_4 (1)	1.5	Phenol	10	100% (20 min)	0.183	11
Fe-N-C-3-800(0.5)	0.4	CIP	20	99% (60 min)	/	12
Fe-C@CNS (0.2)	0.24	CIP	20	100% (60 min)	0.609	13
Fe_3C@NCNT-700 (0.2)	2	Phenol	20	100% (45 min)	0.485	14
Fe@NC-800 (0.2)	0.3	TC	30	95% (60 min)	0.223	15
Co−Fe/NC@GCS (0.2)	0.2	SMX	30	94% (60 min)	0.505	16
$CoFe_{0.8}$@NCNT@CA (0.4)	0.4	TC	40	95% (25 min)	0.803	17
Fe@C-4 (0.1)	0.6	TBBPA		100% (60 min)	1.02	18
FeMn@NC-800 (0.2)	1.68	SMZ	10	97% (30 min)	0.22	19
C-Fe_{ZIF} (1)	13.45	TCAA	10	79% (180 min)	/	20
Fe-SNC-0.2(0.4)	0.22	Phenol	20	99% (10 min)	1.784	This work

C_0: initial concentration of contaminant

The turnover frequency (TOF) was calculated through dividing the reaction rate of pollutant degradation by the catalyst concentration.

TBBPA: tetrabromobisphenol A

SMZ: sulfamethazine

TCAA: trichloroacetic acid

Table S12 Predicted acute (LC50) and chronic (LD50) toxic levels of phenol and its intermediate byproducts using three living organisms: Fish-96 h, Daphnia magna-48 h and Green algae-96 h.

Degraded byproducts	Fish 96h LC_{50} (mg/L)	Daphnid 96h LC_{50} (mg/L)	Green Alge 96h EC_{50} (mg/L)
P (Phenol)	27.7	9.64	2.4
P1	0.095	0.738	0.047
P2	7.01	136	0.736
P3	3.18	36.9	0.242
P4	55979.81	14869.57	2091.37
P5	7.73	25.3	0.962
P6	14.1	115	6.93
P7	491	257	137
P8	66986.86	28903.88	6919.37
P9	7.73	25.3	0.962
P10	0.15	240	94.6
P11	6.08	3.85	4.49
P12	110901.52	51384.62	16512.96
P13	487836.06	189607.45	29465.46
P14	14920475	5647225.5	786367.19

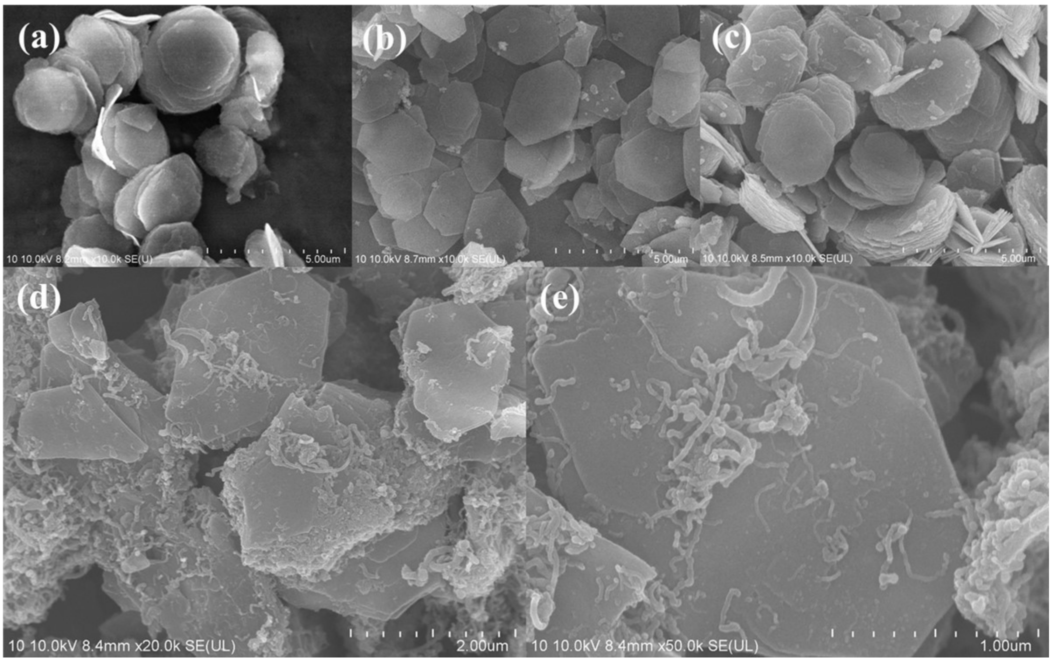

Fig. S1 SEM of (a) ZIF-8, (b) N@ZIF-8, (c) S@ZIF-8, and (d) (e) Fe-NC.

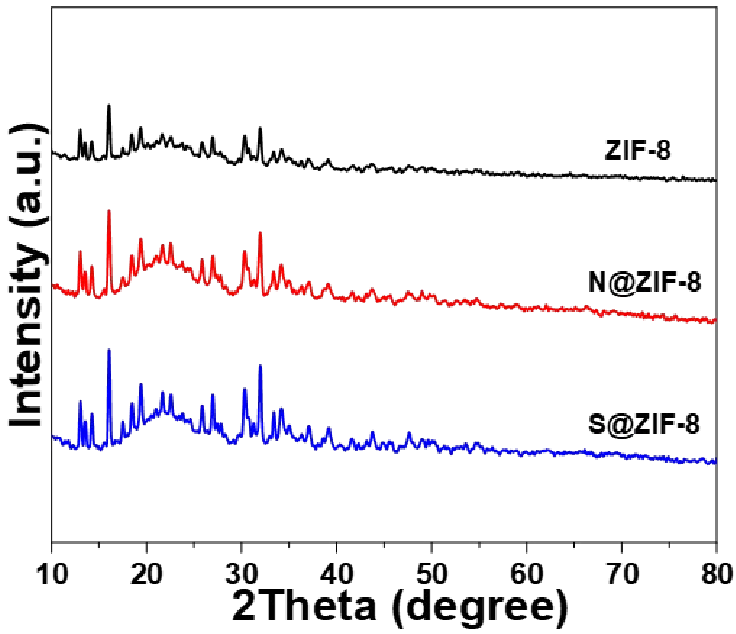

Fig. S2 XRD of ZIF-8, N@ZIF-8 and S@ZIF-8.

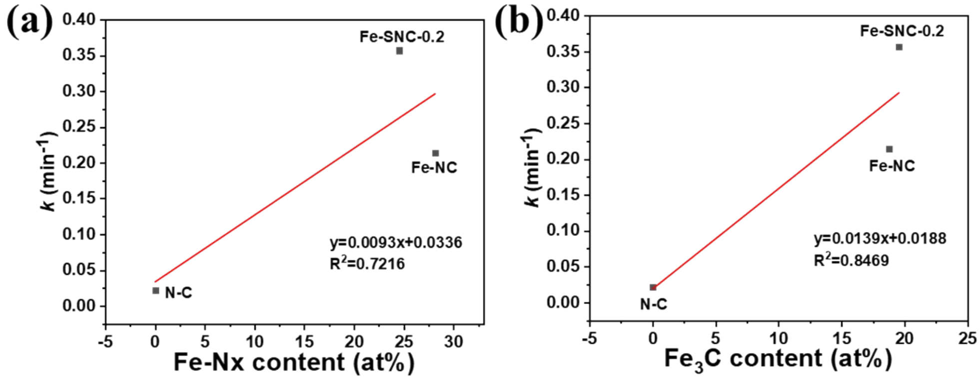

Fig. S3 The relationship between the content of Fe–Nx and Fe_3C and the phenol degradation rate constant (k).

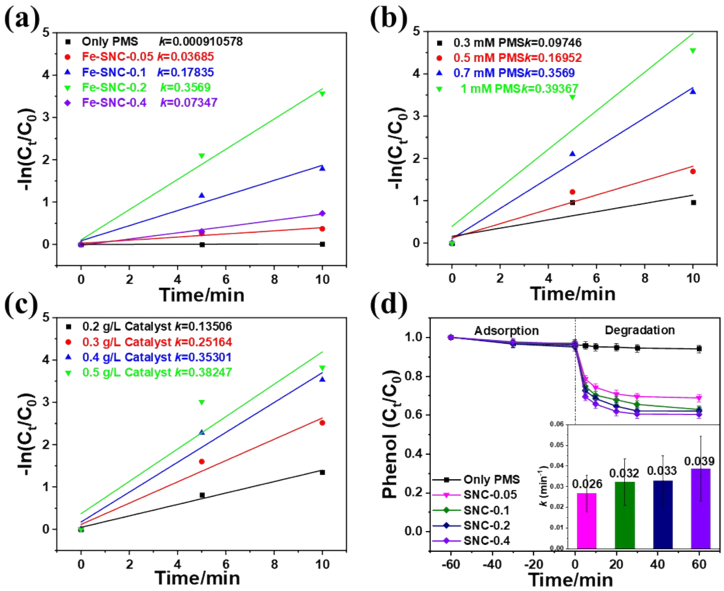

Fig. S4 The corresponding pseudo-first-order kinetic modeling: (a) Iron salt content; (b) PMS concentration, and (c) catalyst dosage. (d) Different concentrations of sulfur doping activated PMS to degrade phenol (Embedded graph: pseudo-first-order rate constants of phenol degradation). Reaction conditions: [PMS] = 0.7 mM, [phenol] = 20 mg/L, [catalyst] = 0.4 g/L, 25 °C, pH=7.

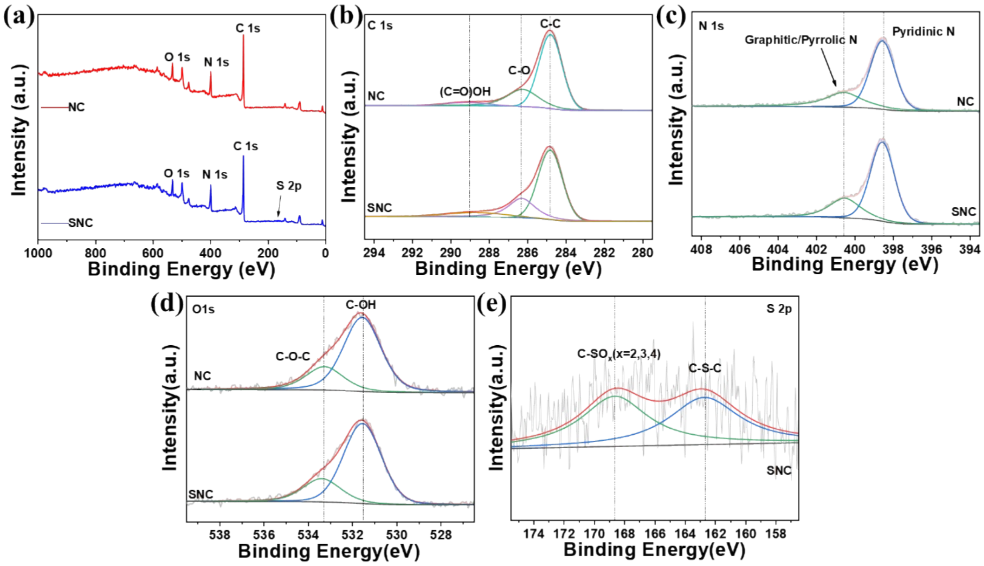

Fig. S5 XPS survey spectra of NC and SNC–0.2 (a). High resolution XPS spectra of (b) C 1s, (c) N 1s, (d) O 1s, and (e) S 2p.

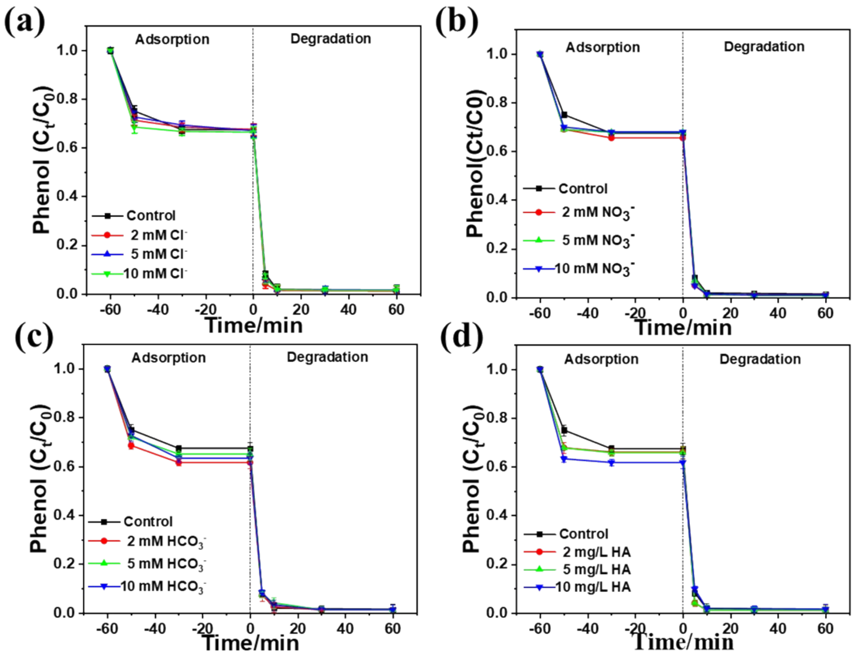

Fig. S6 Effect of anions and natural organic matter on Phenol removal efficiency in Fe-SNC-0.2 degradation system. (a) Cl^-, (b) NO_3^-, (c) HCO_3^-, and (d) HA. Conditions: [PMS] = 0.7mM, [catalyst] = 0.4 g/L, [phenol] = 20 mg/L, [Cl^-] = 2, 5, 10 mM, [NO_3^-] = 2, 5, 10 mM, [HCO_3^-] = 2, 5, 10 mM, [HA] = 2, 5, 10 mg/L, 25 °C, pH=7.

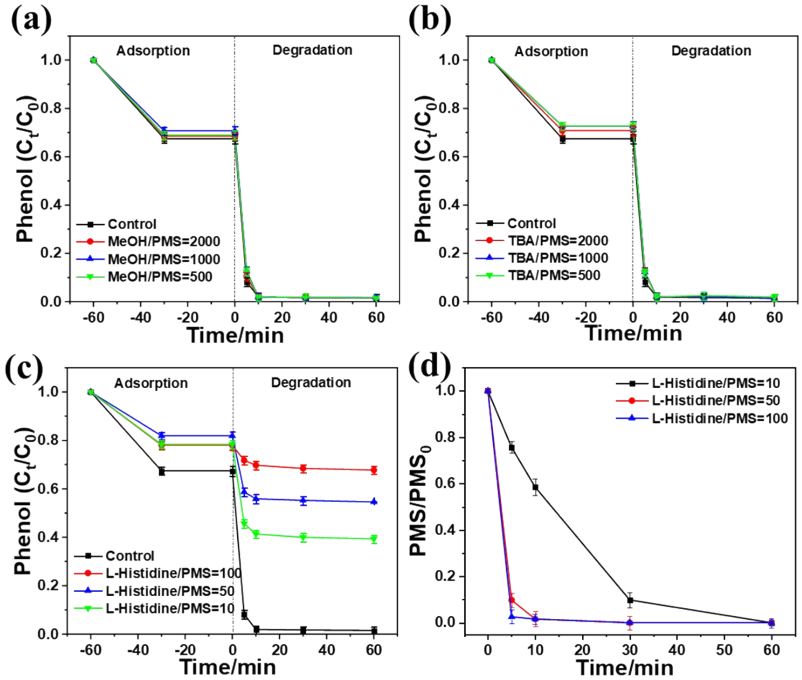

Fig. S7 Removal efficiency of Fe–SNC–0.2 system with different scavengers for Phenol degradation: (a) MeOH, (b) TBA, and (c) L-histidine; (d) PMS consumption. Experimental conditions: [PMS] = 0.7 mM, [phenol] = 20 mg/L, [catalyst] = 0.4 g/L, 25 °C, pH=7.

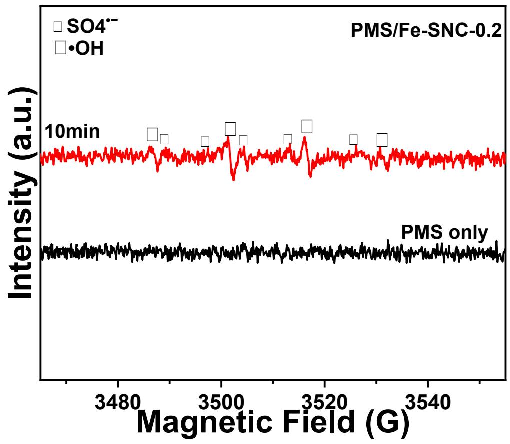

Fig. S8 EPR spectra of DMPO−$SO_4^{\bullet-}$ and DMPO−$^{\bullet}$OH.

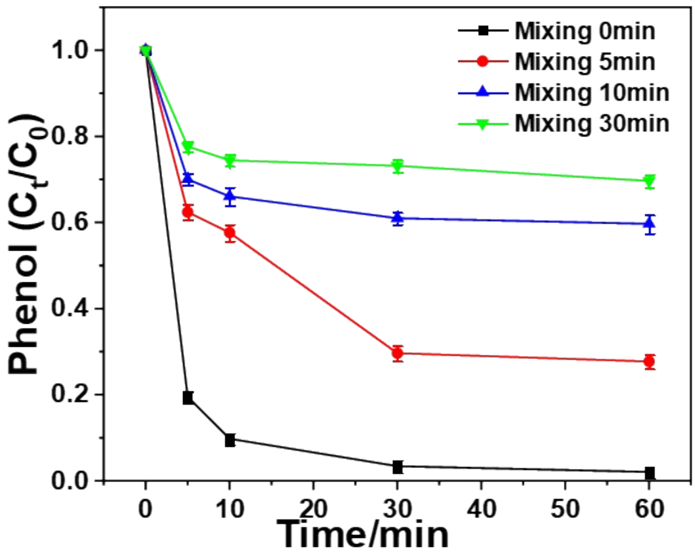

Fig. S9 The degradation efficiency of phenol after premixing Fe-SNC-0.2 with PMS. Conditions: [PMS] = 0.7 mM, [catalyst] = 0.4 g/L, [phenol] = 20 mg/L, 25 ℃, pH=7.

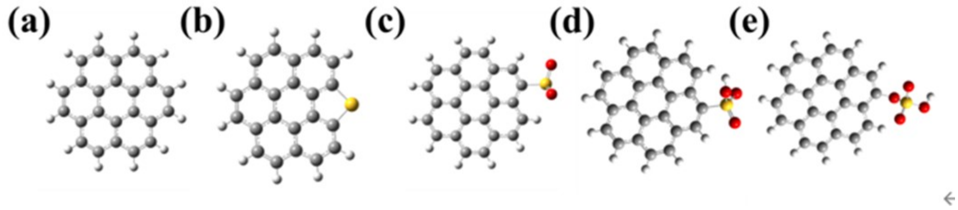

Fig. S10 Several different adsorption configurations of sulfur doping sites: (a) graphene, (b) -C-S-C-, (c) -C-SO_2-, (d) -C-SO_3-, (e) -C-SO_4-.

References

1. H. Xu, X. Sun, H. Yang, J. Cui, J. Wang, Y. Kang, J. Deng and G. Huang, Degradation of aqueous phenol by combined ultraviolet and electrochemical oxidation treatment, *J. Clean.*, **2024**, 436, 140672.

2 Q. Yang, X. Li, S. Zhang, W. Xu, X. Guo, X. Gao and Z. Jia, ZnO hierarchical structures with tunable oxygen vacancies for high performance in photocatalytic degradation of phenol, *J. Mol. Struct.*, **2024**, 1304, 137656.

3. L. Tan, H. Feng, L. Li, H. Lin and J. Xiong, Phenol degradation by a combined hydrogenation and photocatalytic oxidation over the bifunctional Rh/WO_3 catalyst, *J. Environ.*, **2024**, 12, (2),

4. X. Wei, S. Shao, X. Ding, W. Jiao and Y. Liu, Degradation of phenol with heterogeneous catalytic ozonation enhanced by high gravity technology, *J. Clean.*, **2020**, 248,

5. H. Yu, D. Liu, H. Wang, H. Yu, Q. Yan, J. Ji, J. Zhang and M. Xing, Singlet oxygen synergistic surface-adsorbed hydroxyl radicals for phenol degradation in CoP catalytic photo-Fenton, *Chin. J. Catal.*, **2022**, 43, (10), 2678-2689.

6. N. Massalha, S. Dong, M. J. Plewa, M. Borisover and T. H. Nguyen, Spectroscopic Indicators for Cytotoxicity of Chlorinated and Ozonated Effluents from Wastewater Stabilization Ponds and Activated Sludge, *Environ. Sci. Technol.*, **2018**, 52, (5), 3167-3174.

7. W.-L. Wang, M.-Y. Lee, Y. Du, T.-H. Zhou, Z.-W. Yang, Q.-Y. Wu and H.-Y. Hu, Understanding the influence of pre-ozonation on the formation of disinfection byproducts and cytotoxicity during post-chlorination of natural organic matter: UV absorbance and electron-donating-moiety of molecular weight fractions, *Environ. Inter.*, **2021**, 157, 106793.

8. E. C. Wert, F. L. Rosario-Ortiz, D. D. Drury and S. A. Snyder, Formation of oxidation byproducts from ozonation of wastewater, *Water Res.*, **2007**, 41, (7), 1481-1490.

9. Wang, G., Chen, S., Quan, X., Yu, H., Zhang, Y., 2017. Enhanced activation of peroxymonosulfate by nitrogen doped porous carbon for effective removal of organic pollutants. *Carbon*. 115, 730–739.

10. Duan, X., O'Donnell, K., Sun, H., Wang, Y., Wang, S., 2015. Sulfur and nitrogen co-doped graphene for metal-Free catalytic oxidation reactions. *Small*. 11, 3036–3044.

11. Feng, Y., Liao, C., Kong, L., Wu, D., Liu, Y., Lee, P.H., Shih, K., 2018. Facile synthesis of highly reactive and stable Fe-doped g-C_3N_4 composites for peroxymonosulfate activation: A novel nonradical oxidation process. *J. Hazard. Mater.,* 354, 63–71.

12. T. Xiao, Y. Wang, J. Wan, Y. Ma, Z. Yan, S. Huang and C. Zeng, Fe-N-C catalyst with Fe-N_X sites anchored nano carboncubes derived from Fe-Zn-MOFs activate peroxymonosulfate for high-effective degradation of ciprofloxacin: Thermal activation and catalytic mechanism, *J. Hazard. Mater.*, **2022**, 424.

13. H. Chen, R. Chen, S. Yang, D. Ding, X. Li, X. Long, T. Zhao, Y. Du, M. Liu, J. Tan and Y. Chen, Sustainable heterolytic cleavage of peroxymonosulfate by promoting Fe(III)/Fe(II) cycle: The role of in-situ sulfur, *Chem. Eng. J.*, 2022, 446.

14. Wang, C., Kang, J., Liang, P., Zhang, H., Sun, H., Tadé, M.O., Wang, S., 2017. Ferric carbide

nanocrystals encapsulated in nitrogen-doped carbon nanotubes as an outstanding environmental catalyst. *Environ. Sci-Nano*. 4, 170–179.

15. J. Cao, Z. Yang, W. Xiong, Y. Zhou, Y. Wu, M. Jia, H. Peng, Y. Yuan, Y. Xiang and C. Zhou, Three-dimensional MOF-derived hierarchically porous aerogels activate peroxymonosulfate for efficient organic pollutants removal, *Chem. Eng. J.*, **2022**, 427,
16. A. Wang, J. Ni, W. Wang, D. Liu, Q. Zhu, B. Xue, C.-C. Chang, J. Ma and Y. Zhao, MOF Derived Co−Fe nitrogen doped graphite carbon@crosslinked magnetic chitosan Micro−nanoreactor for environmental applications: Synergy enhancement effect of adsorption−PMS activation, *Appl. Catal. B*, **2022**, 319.
17. Y. Wu, Y. Li, T. Zhao, X. Wang, V. I. Isaeva, L. M. Kustov, J. Yao and J. Gao, Bimetal-organic framework-derived nanotube@cellulose aerogels for peroxymonosulfate (PMS) activation, *Carbohydr. Polym.*, 2022, 296.
18. H. Chi, J. Wan, X. Zhou, J. Sun and B. Yan, Fe@C activated peroxymonosulfate system for effectively degrading emerging contaminants: Analysis of the formation and activation mechanism of Fe coordinately unsaturated metal sites, *J. Hazard. Mater.*, **2021**, 419, 126535.
19. Y. He, H. Qin, Z. Wang, H. Wang, Y. Zhu, C. Zhou, Y. Zeng, Y. Li, P. Xu and G. Zeng, Fe-Mn oxycarbide anchored on N-doped carbon for enhanced Fenton-like catalysis: Importance of high-valent metal-oxo species and singlet oxygen, *Appl. Catal. B*, **2024**, 340, 123204.
20. 1. X. Wang, Y. Zhuang and B. Shi, Degradation of trichloroacetic acid by MOFs-templated CoFe/graphene aerogels in peroxymonosulfate activation, *Chem. Eng. J.*, **2022**, 450, 137799.